A Comparison of C-141A Flight Test Measured and Theoretical Vertical Gust Responses

CHARLES T. INGRAM* AND FREDERICK D. EICHENBAUM†
Lockheed-Georgia Company, Marietta, Ga.

The power spectral density function of measured vertical gust velocities for a C-141A flight test and various measures of the resulting response are compared with the theoretical response to an identical one-dimensional vertical gust power spectrum. Plots of the response rms and characteristic frequency obtained by both the spectral and the cross-spectral methods are shown for all major aircraft surfaces responding to vertical gust. In addition, plots of transfer functions, phase angles, and coherency functions vs frequency are given for selected stations. The results show excellent agreement between the theoretical values and the measured data over the frequency range extending from below rigid body motion frequencies up to the 6–7 cps frequency range.

Nomenclature

f = frequency, cycles per second
f_{max} = cutoff frequency for theoretical N_0 integrations
H = experimental transfer function obtained by cross-spectral analysis
i = $(-1)^{1/2}$, imaginary operator for complex variables
N_0 = characteristic frequency
PSD = power spectral density
T = theoretical transfer function and experimental transfer function obtained by spectral methods
V_e = equivalent aircraft velocity, knots
V_T = true aircraft velocity, knots
γ^2 = coherency function
σ = rms incremental response
Φ_g = vertical gust power spectral density
Φ_R = response power spectral density
Φ^+ = cospectral density
Φ^- = quadrature spectral density
ψ = phase lag angle
ω = frequency, radians per second

Subscripts

H = experimental data obtained by cross-spectral analysis
IMAG = imaginary part of complex number
REAL = real part of complex number
T = experimental data obtained by spectral analysis

Matrix notation

$[\ ]$ = rectangular matrix
$\begin{bmatrix} \searrow \end{bmatrix}$ = diagonal matrix
$\{\ \}$ = column matrix
$A_1(\omega)$ = velocity dependent generalized force coefficients
$A_2(\omega)$ = displacement dependent generalized force coefficients
$F_g(\omega)$ = input vertical gust force coefficients
g_n = internal structural damping coefficients
I = inertia load coefficients
$L_g(\omega)$ = input vertical-gust load coefficients
M = generalized masses
$N_1(\omega)$ = velocity-dependent load coefficients
$N_2(\omega)$ = displacement-dependent load coefficients
$q(\omega)$ = generalized displacements
R = transformation from aircraft reference axis system to inertial axis system
$T(\omega)$ = transfer function (i.e., frequency response function)
$\bar{U}'$ = correction vector for the translational velocity of the aircraft axis system origin relative to the inertial axis system
$\bar{V}$ = uncorrected gust velocity vector relative to the gust probe
$\bar{W}'$ = three-component gust velocity vector at the probe measured in an inertial axis system
ϕ' = the normalized modal deflections
$\bar{\omega} \times \bar{l}$ = correction vector for rotation rate of the gust probe about the aircraft reference axis system origin

Submitted February 25, 1969; revision received June 23, 1969. The authors wish to thank those members of the C-141A Aeromechanics Group who contributed to the data reduction and correlation effort. This work was supported by United States Air Force Contract AF 33(600)-42941.

* Dynamics Engineer, Senior. Member AIAA.
† Aircraft Development Engineer, Specialist. Associate Fellow AIAA.

I. Introduction

THE problems encountered in computing the response of a large, swept wing aircraft to continuous atmospheric turbulence are complex, and many of the assumptions made to obtain a workable solution are of uncertain validity. For this reason, a check on the theoretical response may be warranted, if not required, for any new large aircraft. Consequently, an extensive flight test program was undertaken for the C-141A. Numerous flights were made in clear air turbulence for periods of approximately five-minutes duration, during which continuous simultaneous records were made of the gust velocity components and the various aircraft responses. Four of these flights have been analyzed and compared with theoretical predictions for both shear, bending, and torsion loads; as well as three-component accelerations at over a dozen locations on the aircraft. A sample of the results from one such typical flight is presented herein, along with the corresponding theoretical predictions for one-dimensional vertical gust inputs, 1) to demonstrate the ability to measure inflight the gust velocities by means of a pressure sensing probe; 2) to demonstrate the ability to predict the resulting responses with reasonable accuracy; and 3) to provide an indirect check on the theoretical procedures employed.

Table 1 Aircraft geometry and dimensions

Total wing span	= 1919 in.
Fuselage length	= 1588 in. (FS230 to FS1818)
Total horizontal stabilizer span	= 604 in.
Engine locations	= BL 285 and BL 460
Wing sweep angle at $\frac{1}{4}c$	= 23.7° inboard and 25.0° outboard
Horizontal sabilizer sweep angle at $\frac{1}{4}c$	= 25°
Aircraft equipped weight empty	= 132.5 kips

II. Aircraft Description

The C-141A is a heavy logistic transport aircraft with a four turbofan jet engine, high-wing monoplane configuration. The wing has multiple sweep angles, and the horizontal and vertical stabilizer also are swept. The empennage is a cantilever Tee arrangement of vertical stabilizer with a variable incidence horizontal stabilizer. Table 1 contains the basic C-141A dimensions and geometry.

III. Flight Test Instrumentation and Procedures

Continuous in-flight time histories of the parameters necessary to compute three-component gust velocities were obtained by means of a wind-tunnel calibrated pressure sensing probe and special gyros and accelerometers, and were recorded on multiplexed FM tapes for later processing. During the flight test events, pilot inputs to the aircraft were minimal. A description of the gust probe and a derivation of the basic gust velocities data reduction procedures were documented in Ref. 1. In brief, the probe measures dynamic pressure, and vertical and lateral differential pressure. These measurements, along with values of the static pressure and temperature, aircraft angular velocities, translational accelerations obtained from the rate gyros, and linear accelerometers, provide the data needed to compute the gust velocities relative to an earth-fixed axis system.

In addition to gust velocity time histories, continuous simultaneous FM narrow band records were made of bending moments and accelerations at various points on the test aircraft. Calibrated strain gauge bridges employing signals from the front and rear beams of the wing and horizontal stabilizer were used to eliminate the effects of torsion loads on the gauge readings, and the loads on the front and rear beams were combined to give the average bending moments at a particular station. (Although some responses were recorded on both right and left sides of the airplane, only loads for one side of the aircraft are reported herein.)

IV. Data Reduction

General Procedures

The continuous FM multiplexed signals were first converted to continuous individual analog signals, which were digitized at a rate of 40 times per second, converted from voltages to engineering units, and coded for the digital computer data reduction programs. This rate of sampling was chosen to give frequency response functions good to nearly 20 cps. Second, the digitized tapes were input to the digital computer, where final data reduction was performed. The gust time histories were computed with reference to an earth-fixed (inertial) axis system by Eq. (1)

$$\{\bar{W}'\} = [R](\{\bar{V}\} + \{\bar{\omega} \times \bar{l}\}) + \{\bar{U}'\} \tag{1}$$

and low-frequency trend removal performed.[1]

After trend removal, the gust and response time histories were used in the basic data reduction program to compute: 1) the gust *PSD* for the vertical component; 2) the response *PSD*, transfer function, σ and N_0 for both the spectral and cross-spectral methods; and 3) the phase lag angle and coherency function for the cross-spectral method.

Spectral and cross-spectral analyses

The basic spectral and cross-spectral methods of analysis are detailed in NASA Technical Reports.[2,3] The spectral method employs the input and output power spectral densities to calculate a transfer function, rms, and characteristic frequency of the response.

$$T(f) = [\Phi_R(f)/\Phi_g(f)]^{1/2} \tag{2}$$

$$\sigma_T = \left(\int_o^{10} \Phi_R(f)\, df\right)^{1/2} \tag{3}$$

$$N_{0T} = \left(\int_o^{10f^2} \Phi_R(f)\, df\right)^{1/2} \Big/ \sigma_T \tag{4}$$

where the transfer function is described only by magnitude and no phase information is available.

The cross-spectral method uses the cospectra, quadrature spectra, and input spectra to compute not only a transfer function, rms and, characteristic frequency similar to those previously computed, but also a phase lag angle and coherency function, since the transfer function is complex.

$$|H(f)| = [(\Phi^+(f))^2 + (\Phi^-(f))^2]^{1/2}/\Phi_g(f) \tag{5}$$

$$\sigma_H = \left(\int_o^{10} |H(f)|^2 \Phi_g(f)\, df\right)^{1/2} \tag{6}$$

$$N_{0H} = \left(\int_o^{10} f^2 |H(f)|^2 \Phi_g(f)\, df\right)^{1/2} \Big/ \sigma_H \tag{7}$$

$$\psi(f) = \arctan[\Phi^-(f)/\Phi^+(f)], \quad -180° < \psi(f) \leq 180° \tag{8}$$

$$\gamma^2(f) = |H(f)|^2/T^2(f), \; 0 \leq \gamma^2(f) \leq 1.0 \tag{9}$$

In both cases, the required power spectra were calculated in the following sequence and by the techniques of: 1) least squares linear trend removal; 2) prewhitening of gust time histories; 3) auto-covariance (frequently called auto-correlation) computation; 4) cross-covariance computation; 5) shaping the covariance functions by the Hanning process;[4] 6) calculating the power spectral density, cospectral and quadrature spectral density; 7) postdarkening to compensate for prewhitening; and 8) computing transfer functions, σ's, N_0's, phase angles and coherency functions.

Approximately 5.3 min of recorded data (12,780 time history points at 40 points per second) were used to compute spectra at 200 equally spaced frequencies over the range of 0–20 cps. The σ's and N_0's were, however, finally calculated over the range 0–10 cps (Eqs. 3, 4, 6, and 7).

The spectral method gives results based upon the total output spectra, without regard to input source. The cross-spectral method gives data based upon that part of the output that is linearly related to the input, and thus eliminates noise in the output, regardless of source. In this case, the noise is a combination of noise due to instrument errors, digitizing, etc., and aircraft response due to uncorrelated pilot inputs, lateral gust, longitudinal gust, and spanwise varying vertical-gust inputs. Thus, the value of the measured response parameters associated with $T(f)$ and σ_T are too high for uniform vertical gust alone; the values of the response associated with $H(f)$ and σ_H are too low because of the automatic removal of spanwise varying vertical gust response and any other response incoherent with respect to the gust at the probe. Therefore, theoretical rms values and transfer functions should usually fall within the band created by T and H; and σ_T and σ_H. Characteristic frequency values also vary for N_{0T} and N_{0H}, with N_{0T} exceeding the value of N_{0H}, since coherency is lower at higher frequencies than at lower frequencies.

V. Theoretical Predictions

Theoretical response values were calculated using vertical-gust inputs only, for comparison with the test flight results under identical flight conditions as shown in Table 2.

The theoretical model used to represent the aircraft structure consisted of three symmetric rigid body and the first fifteen symmetric flexible modes of vibration. In this case the 15th flexible mode is at 10.9 cps. These are complete aircraft modes of vibration computed by an extension of the Holzer and Myklestad methods[5,6] to the computation of combined bending and torsion modes with six degrees-of-freedom. The mode shapes were based on a system of eighty-one lumped masses connected by flexible shafts having

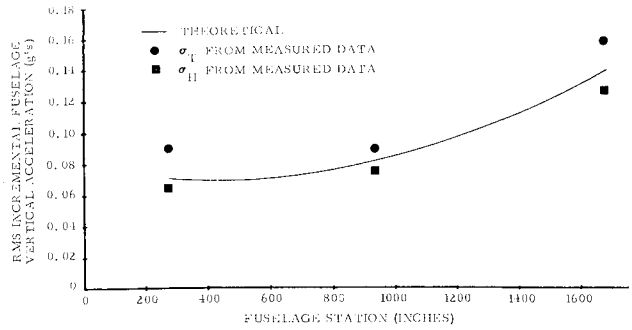

Fig. 1 The rms fuselage accelerations in atmospheric turbulence.

the elastic and geometric properties of the interconnecting structure.

The aerodynamic model used has a panel breakdown corresponding to the structural breakdown, where theoretical circulatory lift coefficients and aerodynamic centers modified to match flight test values were used for each panel. Unsteady lift effects were accounted for by using approximations to the Sears and Theordorsen functions modified for Mach number after a method reported by Wilts[7] and repeated by Theisen and Haas[8] for the corresponding approxi-

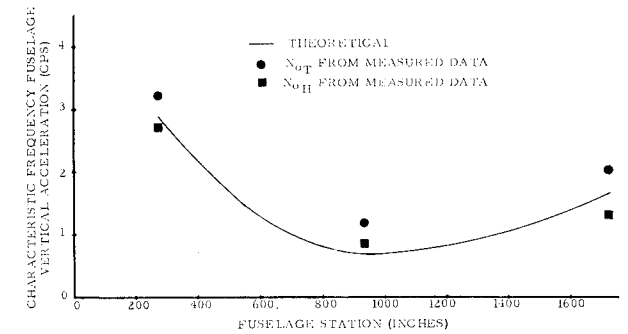

Fig. 2 Characteristic frequencies of fuselage accelerations.

mations[9] to the Kussner and Wagner functions. Since the C-141A has a swept wing and horizontal stabilizer, the cross-flow Mach number, which determines compressibility effects,[5] was used instead of the freestream Mach number when applying the reported corrections derived for an unswept wing.

The aircraft response was thus calculated from the following generalized equation of motion:

$$\left(\left[ig_n\omega_n^2\right]\left[M\right] + \left[\omega_n^2\right]\left[M\right] + \omega^2[M] + i\omega[A_1(\omega)] + [A_2(\omega)]\right)\{q(\omega)\} = \{F_g(\omega)\} \quad (10)$$

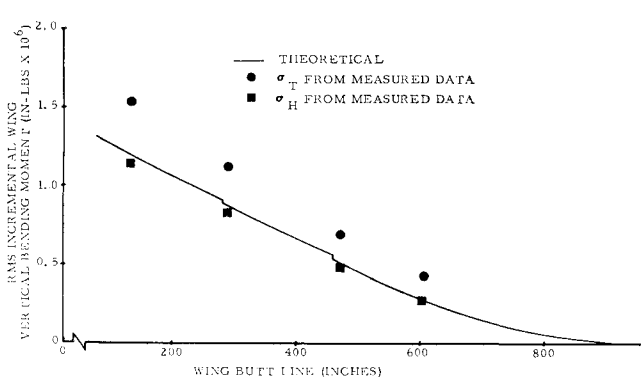

Fig. 3 The rms wing bending moments in turbulence.

Table 2 Theoretical and experimental flight conditions

Altitude (ft)	= 2140
Gross weight (kips)	= 285.0
Fuel weight (kips)	= 125.7 (82% of max)
Cargo weight (kips)	= 26.8 (37% of max)
Mach number	= 0.46
V_e/V_T (knots)	= 292/301

The generalized aircraft displacements obtained from Eq. (10) were next used to compute the transfer functions (i.e., frequency response functions) for the desired loads and accelerations. For loads

$$\{T(\omega)\} = \left(-\omega^2[I] + i\omega[N_1(\omega)] + [N_2(\omega)]\right)\{q(\omega)\} - \{L_g(\omega)\} \quad (11)$$

and for accelerations

$$\{T(\omega)\} = -\omega^2[\phi']\{q(\omega)\} \quad (12)$$

From the real and imaginary parts of the transfer functions, the phase lag angle was computed by

$$\psi(\omega) = \tan^{-1}[T(\omega)_{\text{IMAG}}/T(\omega)_{\text{REAL}}] \quad (13)$$

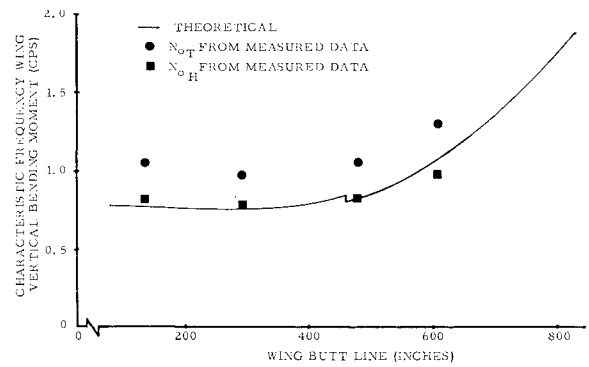

Fig. 4 Characteristic frequencies of wing bending moments.

The rms response and a cutoff frequency were then computed from the equations

$$\sigma = \left(\int_o^{10} |T(f)|^2\Phi_g(f)df\right)^{1/2} \quad (14)$$

$$(0.99\sigma)^2 = \int_o^{f_{\max}} |T(f)|^2\Phi_g(f)\,df \quad (15)$$

The cutoff frequency $f_{\max}$ determined by Eq. (15) finally was used in the following calculation of characteristic frequency

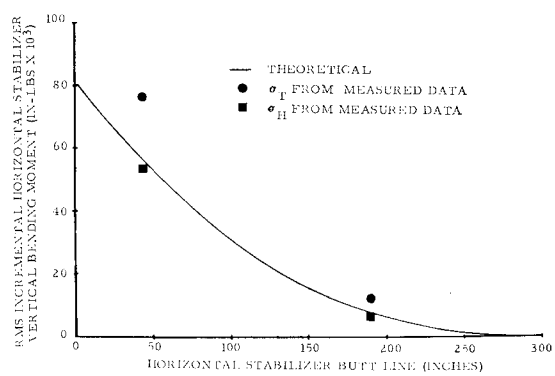

Fig. 5 Horizontal stabilizer rms bending moments in turbulence.

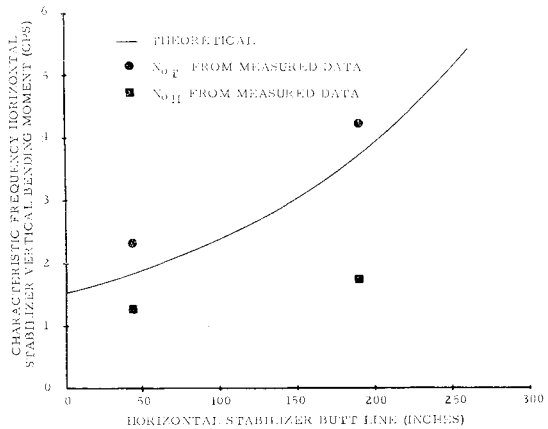

Fig. 6 Characteristic frequencies of horizontal stabilizer bending moments.

to eliminate excessive high frequency, low amplitude influence:

$$N_0 = \left(\int_o^{f_{\max}} f^2 |T(f)|^2 \Phi_g(f) df\right)^{1/2} \Big/ \sigma \qquad (16)$$

VI. Presentation and Comparison of Results

Figures 1–6 show a comparison of the theoretical and experimentally determined values for the rms and characteristic frequency of the response. The theoretical rms values without exception lie between the values computed by the spectral method and the values computed by the cross-spectral method, usually being closer to the cross-spectral values. The characteristic frequency values also correlate well, with no theoretical value deviating greatly from the upper and lower limits set by the experimental data. Trends of the experimental data are reproduced to a fine degree by the trends of the theoretical results.

Figure 7 presents the experimental *PSD* function of the measured vertical gust velocities and is the input spectrum used for the theoretical computations. Breaking over of the spectrum at low frequency, as well as the exponential decline at higher frequencies, stands out clearly. A von Kármán spectrum[3] based upon a scale of turbulence of 700 ft and an rms of 3.2 ft/sec is shown for comparison purposes only and

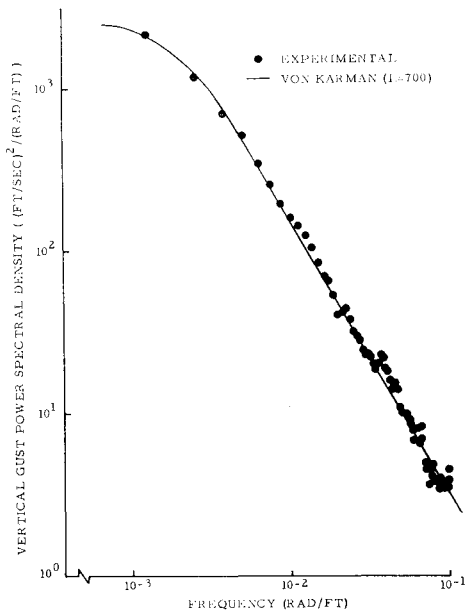

Fig. 7 Flight test measured vertical gust *PSD* with a von Kármán spectrum for comparison.

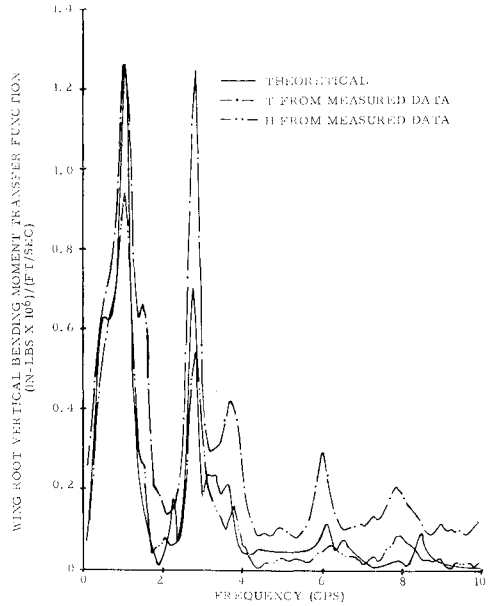

Fig. 8 Comparison of theoretical and experimental transfer functions for wing root bending moment.

was not used in the analysis. The rms of the gust velocity time history and the rms of the power spectrum extrapolated to zero frequency were 3.22 and 3.12 ft/sec, respectively.

Comparisons of transfer functions are shown (Figs. 8, 9, and 10) for a wing root station (WBL 135); a midwing station (WBL 479); and a location near the aircraft center of gravity (FS 935). Theoretical values usually are bounded by the experimental values with the modal representation showing good results even at the higher frequencies. The response peak at approximately 1.8 cps is of special interest, since the wing root and midwing stations show a definite mode at this frequency in the spectral data, whereas little to no response is shown in the theoretical or cross-spectral data. As the first antisymmetric wing bending mode occurs at the frequency, the wing appears to be showing response to lateral gust and spanwise-antisymmetric vertical gust. Averaging the right and left wing responses would remove any antisymmetric response; however, this has not been done. The coherency functions for center of gravity acceleration and midwing vertical bending moment (Fig. 11) are typical of those for the other aircraft responses and show good agreement with the trend estimated by Coleman, Press,

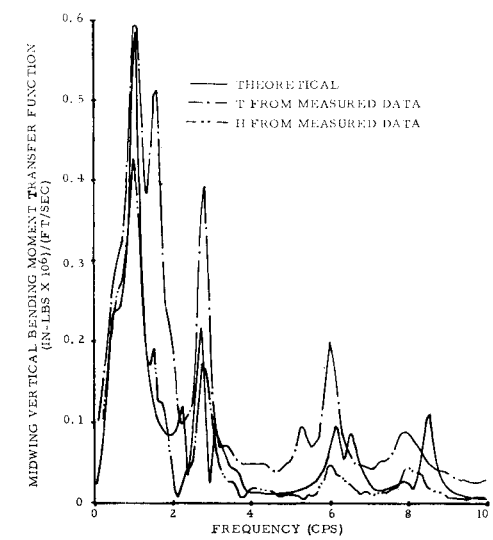

Fig. 9 Comparison of theoretical and experimental transfer functions for midwing bending moment.

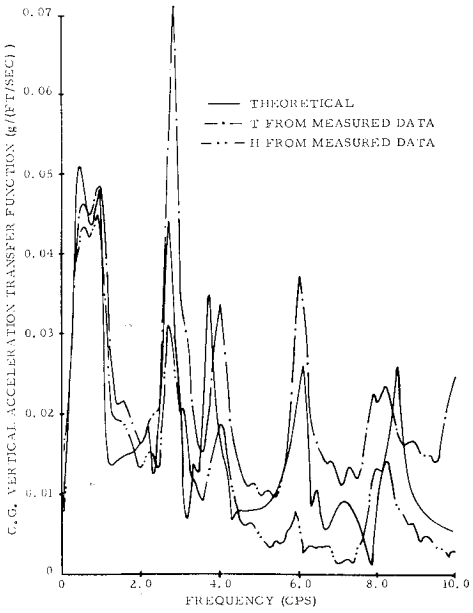

Fig. 10 Comparison of theoretical and experimental transfer functions for center of gravity acceleration.

and Meadows[2] for flight test results of the B-47. This trend (i.e., coherency falling off at higher frequencies) is such that characteristic frequencies computed by the cross-spectral method will be lower than those computed by the spectral method.

Also typical of the additional information obtained by the cross-spectral method are the phase lag angles for the center of gravity acceleration and the midwing vertical bending moment (Fig. 12). Theoretical and experimental phase lag angles compare well not only in trend but also in magnitude to seven cps.

VII. Conclusions

The good comparison between the theoretical results and the cross-spectral experimental data for the flight presented

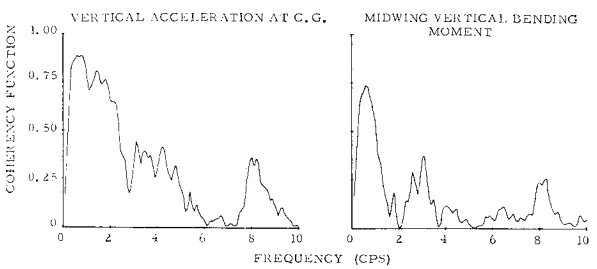

Fig. 11 Coherency function for flight measured center of gravity acceleration and midwing vertical bending moment.

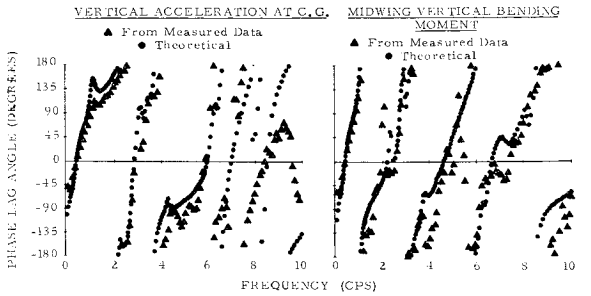

Fig. 12 Phase lag angle for flight measured and theoretical center of gravity acceleration and midwing vertical bending moment.

herein demonstrates that such analytical predictions are possible. The ability to compute and correlate aircraft response with reasonable accuracy on all the major surfaces, not only at the wing root or center of gravity, is of particular significance.

Theoretical transfer function comparisons demonstrate good representations of the aircraft to frequencies of five to six cps and greater, which is far beyond the range of interest in most computations. This excellent comparison also constitutes an indirect check on the validity of the assumptions and theoretical models used.

References

[1] Eichenbaum, F. D., "The Application of Matrix Methods to Clear Air Turbulence Measurement," AIAA Paper 66-967, Boston, Mass., 1966.

[2] Coleman, T. L., Press, H., and Meadows, M. T., "An Evaluation of Effects of Flexibility on Wing Strains in Rough Air for a Large Swept-Wing Airplane by Means of Experimentally Determined Frequency-Response Functions with an Assessment of Random-Process Techniques Employed," TR-R-70, 1960, NASA.

[3] Houbolt, J. C., Steiner, R., and Pratt, K. G., "Dynamic Response of Airplanes to Atmospheric Turbulence Including Flight Data on Input and Response," TR-R-199, June 1964, NASA.

[4] Blackman, R. B. and Tukey, J. W., *The Measurement of Power Spectra,* 1st ed., Dover, New York, 1958.

[5] Bisplinghoff, R. L., Ashley, H., and Halfman, R. L., *Aeroelasticity,* 1st ed., Addison-Wesley, Cambridge, Mass., 1955.

[6] Scanlan, R. H. and Rosenbaum, R., *Introduction to the Study of Aircraft Vibration and Flutter,* 1st ed., Macmillian, New York, 1951,

[7] Wilts, C. H., "Aerodynamic Forces in Analog Computation," TR-116, Sept. 1959, California Institute of Technology Computing Center, Pasadena, Calif.

[8] Theisen, J. G. and Haas, J., "Turbulence Upset and Other Studies on Jet Transports," *Journal of Aircraft,* Vol. 5, No. 4, July-Aug. 1968, p. 350.

[9] Foss, K. A. and McCabe, W. L., "Gust Loading of Rigid and Flexible Aircraft in Continuous Atmospheric Turbulence," TR-57-704, Jan. 1958, Wright Air Development Center, Dayton, Ohio, pp. 115–116.